The Journal of Engineering

IET International Radar Conference (IRC 2018)

IET Journals
The Institution of Engineering and Technology

Prospects of FMCW-based frequency diverse array radar

eISSN 2051-3305
Received on 20th February 2019
Accepted on 3rd May 2019
E-First on 7th October 2019
doi: 10.1049/joe.2019.0458
www.ietdl.org

Ramazan Çetiner[1], Çağrı Çetintepe[2], Şimşek Demir[2], Altunkan Hizal[1] ✉

[1]*Radar and Electronic Warfare Systems, Aselsan, Ankara, Turkey*
[2]*Middle East Technical University, EEED, Ankara, Turkey*
✉ *E-mail: ahizal@aselsan.net*

Abstract: The linear frequency modulated (LFM) frequency modulated continuous wave (FMCW)-based frequency diverse array (FDA) radar concept is investigated in detail. The radar operates as a linear pulsed FMCW/FDA in the transmission (TX) mode while it operates as a pulsed FMCW/phased array (PA) in the receiving mode. The issues such as low signal-to-noise ratio (SNR) of FDA, the time-angle scanning and time-range ambiguities are studied. It is shown that the local instantaneous frequency bandwidth is much smaller than the radio frequency (RF) deviation of LFM. Positive and negative slope TX/RF locations offer frequency diversity. Time domain and frequency domain signal processings are described. A Ku band direct digital synthesis-based FMCW/FDA radar example based on the cumulative detection scheme is given and compared with an equivalent FMCW/PA radar.

1 Introduction

The frequency diverse array (FDA) was first introduced in [1] and developed in [2]. The frequency modulated continuous wave (FMCW)-based FDA was introduced in [3–5]. The FDA effect was obtained by applying the chirp signal to the elements of a linear uniform array by progressive time delays T_ℓ, which was restricted to small values (< 1 ns) to reduce the size of the array. Here, we propose to use a direct digital synthesis (DDS)-based FMCW/FDA to remove this restriction. T_ℓ is a major parameter, which determines the chirp radio frequency (RF) frequency band width (fBW) Δf. If the peaks and nulls of the adjacent spectral components of the Fourier spectrum ($\mathcal{FS}$) of the FDA waveform coincide, we have the spectral orthogonality (SO) and $\mathcal{K} = \Delta f T_\ell \in \mathbb{Z}$. We choose $\mathcal{K} = 2$. The SO shapes the $\mathcal{FS}$ for a better range and Doppler processing. The chirp length and slope are τ and $\mu_\mathrm{f} = \pm \Delta f/\tau$, respectively. The base band beat frequency (BF) for the radar range delay $T_\mathrm{do} = 2R_\mathrm{o}/c$; c is the velocity of light, is $f_\mathrm{bo} = \mu_\mathrm{f} T_\mathrm{do}$. The issues such as range-angle coupling, low-SNR problem, and range angle time ambiguities are discussed. Methods are proposed to solve these problems. Positive and negative slope linear frequency modulated (LFM) cases are considered. The local positions of the transmission (TX)/RF for ±slopes for an angle are different, which provides a frequency diversity feature. Moreover, the bandwidths associated with a particular angle are much smaller than Δf. The FDA concept is used in TX only. In receiving (RX) digital beam forming (DBF) for phased array (PA) is proposed. A multiple-pulsed FMCW/FDA radar in Ku-band is designed to illustrate the basic concepts such as fast scanning of angular space in slow time. The SNR for FDA per angle is M times lower than the corresponding SNR for PA, where M is the number of elements of the array in the FDA part. The low SNR of FDA radar is compensated by angular scanning property in slow time, the cumulative detection scheme and temporal decorrelation of the target. Also, a comparison between two equivalent FMCW/FDA and FMCW/PA radars is made.

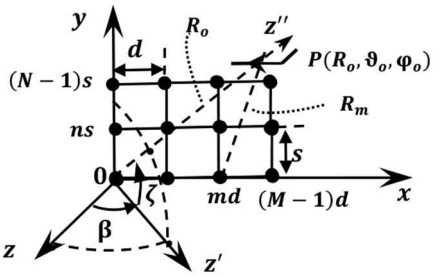

Fig. 1 *Linear array with far field point*

2 Theory

A linear planar array with M equidistant elements is shown in Fig. 1. The elements are fed by DDS oscillator voltages

$$V_\mathrm{m}(t) = a_\mathrm{m} \exp\left[\mathrm{j}\left(\omega_\mathrm{o} t'_\mathrm{m} + \frac{\mu}{2} t'^2_\mathrm{m}\right)\right] \cdot P(t'_m, \tau) \tag{1}$$

where $t'_\mathrm{m} = t - mT_\ell$, $P(t, \tau) = 1$ for $0 \le t \le \tau$, 0 elsewhere.

$\mu = 2\pi\mu_\mathrm{f}$. $\omega_\mathrm{o} = 2\pi f_\mathrm{o}$ is the carrier frequency, a_m is the element weight. The frequency is $\omega(t) = \omega_\mathrm{o} + \mu t$; for the + slope, i.e. $\mu > 0$. The TX field at point P is expressed by

$$E_\mathrm{TX}(t') \cong \frac{F_\mathrm{N} f_\mathrm{e}}{R_\mathrm{o}} P(t', \tau) \mathrm{e}^{\mathrm{j}\left(\omega_\mathrm{o} t' + (\mu/2) t'^2\right)} \sum_{m=0}^{M-1} a_m \mathrm{e}^{\mathrm{j}m\gamma(t')} \tag{2}$$

where f_e is the wide band element pattern. $t' = t - T_\mathrm{do}/2$ is the retarded time. F_N is the y-array with N elements with spacings s is a corporate connection of N FDA x-arrays

$$F_N \cong \sum_{n=0}^{N-1} a_n \mathrm{e}^{\mathrm{j}n2\pi(s/\lambda_\mathrm{o})\sin\vartheta_\mathrm{o}\sin\varphi_\mathrm{o}} \tag{3}$$

The phase factor $\gamma(t')$ for the + slope can be expressed by

$$\gamma^+(t') = -2\pi\nu_\mathrm{o}\left(\frac{t'}{T_\mathrm{f}} + 1\right) + m\,\pi\mu_\mathrm{f}\left(\frac{\nu_\mathrm{o}}{f_\mathrm{o}}\right)^2 = u + \Delta u \tag{4}$$

$$\nu_\mathrm{o} = f_\mathrm{o} \cdot T_\ell - \frac{d}{\lambda_\mathrm{o}} \sin\vartheta_\mathrm{o} \cos\varphi_\mathrm{o} > 0 \tag{5}$$

where λ_o is the wavelength and $T_\mathrm{f} = f_\mathrm{o}/\mu_\mathrm{f}$. We have $u + \Delta u \cong u$ as $u_\mathrm{o} \gg \Delta u_\mathrm{o}$, where $u_\mathrm{o} = u - \mathrm{IP}\{u/(2\pi)\} \cdot 2\pi$ and that $\Delta u_\mathrm{o} = \Delta u - IP\{\Delta u/(2\pi)\} \cdot 2\pi$. IP is the integer part. Then,

$$\gamma^{+}(t') \cong -2\pi\nu_{\rm o}(t'/T_{\rm f}+1) \tag{6}$$

For $a_m = 1$, the summation in (2) becomes

$$F_M(\gamma) = {\rm e}^{{\rm j}(M-1)\gamma/2}\sin(M\gamma/2)/\sin(\gamma/2) \tag{7}$$

The time of arrival of the peak TX signal at P (Fig. 1) can be obtained from (5) by setting $\gamma(t'_{\rm o}) = 2\pi p$; $p \in \mathbb{Z}$. Thus

$$t_{\rm o}^{'+} = T_{\rm f}(-p/\nu_{\rm o} - 1) \tag{8}$$

Since $0 \le t'_{\rm o} \le \tau$, we can show that there will be $\mathscr{K} = 2$ peaks in τ with $p = -{\rm CE}\{\nu_{\rm o}\}$ and $p = -{\rm CE}\{\nu_{\rm o}\} - 1$, where CE stands for the ceiling integer. For $M\gamma/2 = \pi p$, $F_M(\gamma)$ makes nulls, which leads to the null-to-null time beam width (TBW)

$$T_{\rm nn} = 2|T_{\rm f}|/(M\nu_{\rm o}) \cong 2\tau/(\mathscr{K}\cdot M) \tag{9}$$

since $f_{\rm o}T_\ell \gg d/\lambda_{\rm o}$. As the TX chirp signal arrives at the mth element at $t = mT_\ell$, the array is filled up at a time

$$T_{\rm fill} = (M-1)T_\ell \tag{10}$$

The LFM chirps applied to antenna elements are shown in Fig. 2. The fill time of the array should satisfy $T_{\rm fill} \ll \tau$.

For the - slope, i.e. $\mu < 0$, $\omega(t) = \omega_{\rm o} + \Delta\omega + \mu t$

$$\gamma^{-}(t') \cong -2\pi\nu_{\rm o}\cdot(t'/T_{\rm f} + 1 + \eta); \quad \eta = \Delta f/f_{\rm o} \tag{11}$$

$$t_{\rm o}^{'-} = T_{\rm f}(-p/\nu_{\rm o} - 1 - \eta) \tag{12}$$

The rate of rotation of the peak from (8) or (12) is

$$\Omega_\vartheta = \frac{\partial\vartheta_{\rm o}}{\partial t} = \frac{\nu_{\rm o}^2}{-pT_{\rm f}(d/\lambda_{\rm o})\cos\vartheta_{\rm o}\cos\varphi_{\rm o}} \cong \frac{{\rm sign}(\mu_{\rm f})\mathscr{K}}{\tau(d/\lambda_{\rm o})\cos\vartheta_{\rm o}\cos\varphi_{\rm o}} \tag{13}$$

The RX signal with TX/RX isolation is obtained by mixing the received echo by a coherent local oscillator (LO) chirp as in (1) with duration $\tau_{\rm LO} \ge \tau + T_{\rm do} + T_{\rm fill} - T_{\rm LO}$, where $T_{\rm LO}$ is the time offset for reducing $f_{\rm bo}$. The base band IF signal is similar to that of the classical FMCW signal but with the FDA modulating waveform (7). Thus, the base band RX voltage is

$$V^{+}(t') \cong V_{\rm o}\,{\rm e}^{{\rm j}\psi(t')}P(t',\tau)\sum_{m=0}^{M-1} a_m{\rm e}^{{\rm j}m\gamma^{+}(t')} \tag{14}$$

where $t' = t - T_{\rm do}$ and $\psi(t') \cong \omega_{\rm b}t'$ with the effective BF $\omega_{\rm b} = \omega_{\rm bo} + \omega_{\rm do}$, where $\omega_{\rm bo} = \mu(T_{\rm do} - T_{\rm LO})$ is the BF and $\omega_{\rm do} = 2\omega_{\rm o}v_{\rm tg}/c$ is the Doppler frequency (DF) for a target with outgoing velocity $v_{\rm tg} > 0$. $V_{\rm o}$ is the complex amplitude depending on TX and RX functions of the radar and propagation path. The Fourier transform ($\mathscr{F}\mathscr{T}$) of $V^{+}(t')$ can be expressed by

$$\tilde{V}^{+}(\omega) = {\rm e}^{-{\rm j}\omega T_{\rm do}}V_{\rm o}\tau\sum_{m=0}^{M-1} a_m{\rm e}^{-{\rm j}(m2\pi\nu_{\rm o}+(\bar{\omega}\tau/2))}\frac{\sin(\bar{\omega}\tau/2)}{\bar{\omega}\tau/2} \tag{15}$$

where $\bar{\omega} = \omega - \omega_{\rm b} + m\omega_\ell$; $\omega_\ell = 2\pi\nu_{\rm o}/T_{\rm f} = 2\pi f_\ell$. If the peak of a spectral component is to coincide with the $\mathscr{K}-$th null of the adjacent one, we have $\omega_\ell \cong 2\pi\mathscr{K}/\tau$, which yields $\Delta f\cdot\nu_{\rm o}/f_{\rm o} = \mathscr{K}$. Since $f_{\rm o}\cdot T_\ell \gg d/\lambda_{\rm o}$, $\Delta f\cdot T_\ell = \mathscr{K} = 2$ for the SO. Thus, $\mathscr{F}\mathscr{S}$ fBW $f_{\rm BW}$ can be expressed by $f_{\rm BW} = (M-1)f_\ell + 2/\tau \cong 2M/\tau$. If two targets are separated by $\Delta R_{\rm o}$ such that the corresponding $\mathscr{F}\mathscr{S}$ are just adjacent to each other, we should have the BF increment $\Delta f_{\rm bo} = f_{\rm BW}$, which yields the range resolution spatial increment $\Delta R_{\rm o} = \tau\cdot f_{\rm BW}\cdot c/(2\Delta f) \cong 2M\cdot c/(2\Delta f)$. It is seen that $\Delta R_{\rm o}$ increases by a factor of $2M$ compared to the classical FMCW radar

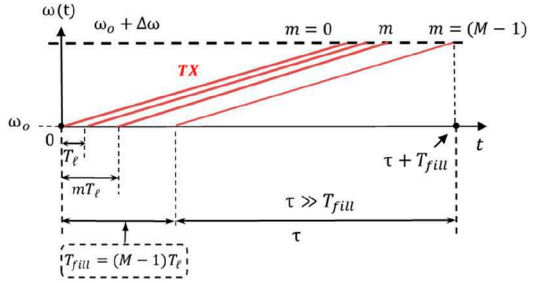

Fig. 2 *LFM chirps for antenna elements*

having the same Δf. For - slope, $m2\pi\nu_{\rm o}$ in (15) is replaced by $m2\pi\,\nu_{\rm o}(1+\eta)$. The centre frequency of the mth spectral is $\bar{\omega}_{mc} = \pm\omega_{\rm bo} + \omega_{\rm do} - m\omega_\ell$.

3 Numerical example

We choose $f_{\rm o} = 17.4\,{\rm GHz}$, $M = 13$, $N = 4$, $d/\lambda_{\rm o} = s/\lambda_{\rm o} = 0.5$, $T_\ell = 2\,{\rm ns}$, $\tau = 1\,{\rm ms}$, and $\Delta f = \Delta f^{\rm FDA} = 1\,{\rm GHz}$. Then, $\mathscr{K} = 2$, $f_\ell = \mathscr{K}/\tau = 2\,{\rm kHz}$, $\mu_{\rm f} = 1\,{\rm GHz}/\mu{\rm s}$, $f_{\rm o}\,T_\ell = 34.8$, $T_{\rm f} = 17.4\,{\rm ms}$, $T_{\rm fill} = 24\,{\rm ns}$, $\eta = 5.75\%$, $f_{\rm BW} = 26\,{\rm kHz}$, and $\Delta R_{\rm o} = 3.897\,{\rm m}$. The waveforms for $a_m = 1$, $\varphi_{\rm o} = 0°, 180°$ and $0° \le \vartheta_{\rm o} \le 50°$, are shown in Figs. 3 and 4. The time and range periods of the waveforms are $\mathscr{T}_{\rm p}^{\rm FDA} = T_{\rm f}/\nu_{\rm o} \cong 1/f_\ell = 500\,\mu{\rm s}$ and $\mathscr{R}_{\rm p}^{\rm FDA} = c\mathscr{T}_{\rm p}^{\rm FDA} = 150\,{\rm km}$, respectively. The beam widths are $\vartheta_{\rm BW}^{az}(0°, 50°) = \{7.8°, 12°\}$. The FDA pattern rotates in (clockwise (CW), counter-clockwise (CCW)) for $(+, -)$ chirp slopes. For $\varphi_{\rm o} = \{0°, 180°\}$ and $\vartheta_{\rm o} = 0° \to 50°$, $T_{\rm nn} = \{76.9 \to 77.7, 76.9 \to 76.1\}\mu{\rm s}$. The difference of the time of arrivals for ±slopes is given by $\Delta t_{\rm o} = t_{\rm o}^{'+} - t_{\rm o}^{'-} = -|T_{\rm f}|(2\,p/\nu_{\rm o} + 2 + \eta)$, which can be solved for $\sin\vartheta_{\rm o}\cos\varphi_o$. We can determine $\vartheta_{\rm o}$ by the axes transformation from x, y, z to $\bar{x} = y$, $\bar{y} = z$, $\bar{z} = x$. Then we have $\sin\vartheta_{\rm o}\cos\varphi_{\rm o} = \cos\bar{\vartheta}_{\rm o}$. In the azimuth plane, i.e. in an $xz = \bar{y}\bar{z}$-plane, we have $\varphi_{\rm o} = 0°$ and $\bar{\varphi}_{\rm o} = 90°$ for which $\vartheta_{\rm o} = \bar{\vartheta}_{\rm o} - 90°$. The sum of the time of arrivals for ±slopes is $\Sigma t_{\rm o} = t_{\rm o}^{'+} + t_{\rm o}^{'-} = 4R_{\rm o}/c + |T_{\rm f}|\eta$, which is a function of range only. For a single target these methods may work. However, the range resolution in the time domain ($\mathscr{T}\mathscr{D}$) is not possible since $\Delta R_{\rm o}(T_{\rm nn}) = cT_{\rm nn}/4$ is very large. Thus, the range should be found in the $\mathscr{F}\mathscr{T}$ domain. Similarly, the angle determination based on $\Delta t_{\rm o}$ for targets spaced in $\Delta R_{\rm o}(T_{\rm nn})$ is not convenient and they should be determined by the RX beams. Two targets at $R_{o1}, \vartheta_{\rm o1}, \varphi_{o1}$ and $R_{\rm o2}, \vartheta_{\rm o2}, \varphi_{\rm o2}$ may have the same time of arrivals, i.e. $t_{\rm o1}^{'+} = t_{\rm o2}^{'+}$. Then, $\Delta R_{\rm o12}^{+} = R_{\rm o1} - R_{\rm o2} = T_{\rm f}(p_1/\nu_{\rm o1} - p_2/\nu_{\rm o2})$. At $\vartheta_{\rm o} = \{0°, 50°\}$, $\varphi_o = 0°$, $\{\vartheta_{\rm o1}, \vartheta_{\rm o2}\} = \vartheta_{\rm o} \mp \vartheta_{BW}^{az}/2$, $\Delta R_{\rm o12}^{+} = \{5.12, 5.26\}{\rm km}$. At $\varphi_{\rm o} = 180°\Delta R_{\rm o12}^{+} = \{-5.12, -5.14\}{\rm km}$. For the - slope $\Delta R_{\rm o12}^{-} = -\Delta R_{\rm o12}^{+}$. The BF carrier of the modulating FDA envelope in each case is proportional only to $T_{\rm do}$ and the Doppler of the target. The $\mathscr{F}\mathscr{T}$ $\tilde{V}^{+}(\omega)$ is shown in Fig. 5. The spectrals shift to the right ($\to +f$) for $m = 0, M-1$. The parameters are so chosen that the $\mathscr{F}\mathscr{S}$ has a stable shape for $\vartheta_{\rm o} = 0° \to 50°$. The leading and trailing edge slopes are that of the spectrals for $m = M-1$ and $m = 0$, respectively. The shift in the $\mathscr{F}\mathscr{S}$ is $\Delta f_{\rm sm} = m(d/\lambda_{\rm o})\sin\vartheta_{\rm o}\cos\varphi_{\rm o}/T_{\rm f}$. For $\varphi_{\rm o} = 0°$, $m = 12$, $\vartheta_{\rm o} = 50°$, and $\Delta f_{\rm sm} = 0.264\,{\rm kHz}$. As $\Delta f_{\rm sm}/f_{\rm BW} = 0.01$, a leading edge measurement causes an error of 3.96 cm. For the - slope, the trailing edge of the $\mathscr{F}\mathscr{S}$ shifts to the left ($-f \leftarrow$) in $\varphi_{\rm o} = 0°$ plane. The $\mathscr{F}\mathscr{S}$ shifts in the opposite direction for $\varphi_{\rm o} = 180°$.

The $\mathscr{F}\mathscr{S}$ for two targets separated by $\Delta R_{\rm o}(\mathscr{F}\mathscr{T}) = 3.897\,{\rm m}$ is shown in Fig. 6. The BF due to the range and +DF due to the – velocity (closing in target) shifts the spectra as shown in Fig. 7. By measuring $f_{\rm b\pm}$ we can obtain both $f_{\rm bo}$ and $f_{\rm do}$, which enables us to find both $R_{\rm o}$ and $v_{\rm tg}$. For $R_{\rm o} = 1.5\,{\rm km}$, $T_{\rm do} = 10\,\mu{\rm s}$, and

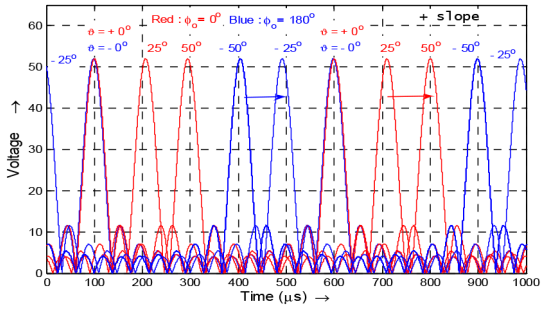

Fig. 3 *Retarded time of arrivals for + slope;* $\varphi_o = 0°, 180°$

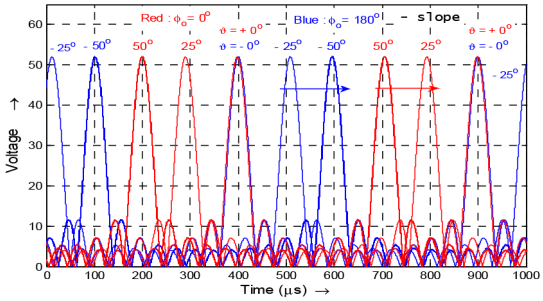

Fig. 4 *Retarded time of arrivals for - slope;* $\varphi_o = 0°, 180°$

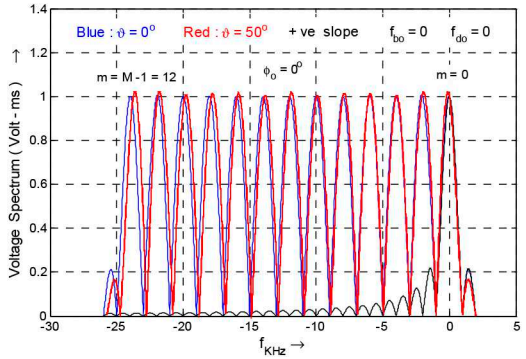

Fig. 5 *$\mathcal{FT}$ spectrum for + slope and* $\vartheta_o = 0°$ & $50°$; $\varphi_o = 0°$

$f_{bo} = 10$ MHz. Using direct digital synthesizer local oscillator (DDSLO) with $T_{LO} = 9\,\mu$s we have $f_{bo} = \mu_f \cdot (T_{do} - T_{LO}) = 1$ MHz. The measurement accuracy depends on SNR $= E_o/\eta_o$, where E_o is the energy of the FDA waveform and $\eta_o = kT_s$ is the noise spectrum density. E_o is the area of the square of $\mathcal{FS}$, which can be shown to be $E_o \cong MV_o^2\tau = 13\,\text{mJ}/V_o^2$. Finding the coherent average of $\mathcal{FT}$ recovers E_o. This is a matched filtering in $\mathcal{FT}$ domain. For Swerling I (SW I) targets Doppler filters (DFL) can be formed by applying another $\mathcal{FT}_D$ for N_- ± chirps. This is the 2D $\mathcal{FT}$ for FMCW radars [6]. N_- radar pulses are shown in Fig. 8 where the time gap $T_g > T_{do}$ is required for dechirping and per pulse sampling.

The general phase term of the nth pulse is expressed by $\psi_n[t' + (n-1)T] = \omega_{bn}t' + (n-1)\omega_{do} + \alpha_n$ for $t' \in [0, \tau]$, where $\omega_{bn} = \omega_{bo} + \omega_{do} + \mu(n-1)v_{tg}T_p$ is the effective BF and $\alpha_n = -\Delta\varpi_{bn}[2R_o/c + (n-1)vT/c]$. We have $\psi \to \psi_n$ and $\tilde{V}^+(\omega) \to \tilde{V}^+(\omega - \omega_{bn})$. $\mathcal{FT}_D$ and $\tilde{V}^+(\omega - \omega_{bn})$ can be realised by a discrete $\mathcal{FT}$; $\omega = \omega_i$; $i = 1, \ldots, i_{max}$ where i_{max} is the number of time and $\mathcal{FT}$ samples

$$\breve{V}_{\mathcal{k}i} = \sum_{n=0}^{N_- - 1} \tilde{V}(\omega_i - \omega_{bn})\, e^{-j2\pi(n-1)\mathcal{k}/N_- - j\alpha_n} \tag{16}$$

which forms for $\mathcal{k} = 0, 1, \ldots, N_- - 1$, N_- DFL with period $2\pi/T$, null-to-null fBW $4\pi/(N_- \cdot T)$ and the centre frequency

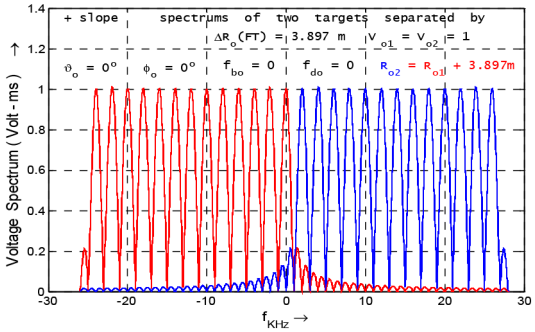

Fig. 6 *$\mathcal{FT}$ spectrum of two targets separated by* ΔR_o

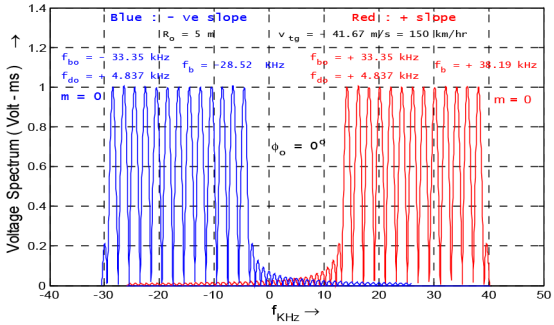

Fig. 7 *$\mathcal{FT}$ spectra with beat and Doppler frequencies*

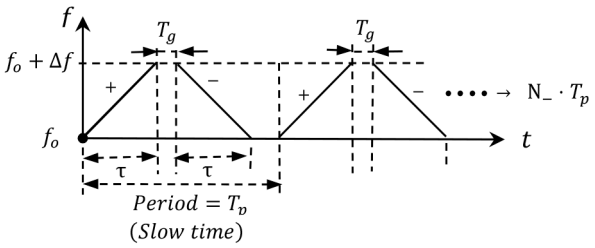

Fig. 8 *Periodic coherent ± slopes* N_- *radar pulses*

$\omega_{c\mathcal{k}} = 2\pi\mathcal{k}/(N_- \cdot T)$. The inclusion of α_n means, we form velocity compensated DFL. The required velocity estimation can be achieved either from the ±slope range $\mathcal{FT}$ or forming the complex signal $V_{cn}(t') = V_n(t') + j\hat{V}_n(t')$, where $\hat{V}_n(t')$ is the Hilbert transform of $V_n(t')$. If Φ_n is the phase of $V_{cn}(t')$, we have $\Delta\Phi_n = \psi_{n+1} - \psi_n \cong \omega_{do}T$.

4 Simulation of a Ku band radar

The TX/RX antennas are well separated for good isolation. The antenna's dimensions are 10.34 cm × 2.6 cm. The antenna patterns are shown in Fig. 9. $\vartheta_{BW}^{az} = 7.8°$, $\vartheta_{BW}^{el} = 26.3°$ for $\zeta = 0$. The antenna gain is $G_A = 22$ dB. The parameters other than those given in Section 3 are as follows: $N_-^{FDA} = 8$ coherent pairs of ±pulses form a burst. $T_g = 250\,\mu$s and $T_p = 2500\,\mu$s. The duty cycle is 80%. The number of bursts is $n_-^{FDA} = 21$. The radar range equation is

$$\text{SNR} = \frac{E_{ot}}{r_E kT_s} \cdot \frac{G_A^2 \sigma_s \lambda_o^2 L_t L_a}{(4\pi)^3 R_o^4} = \frac{D_1 L_x}{I_n G_i G_{div}} \tag{17}$$

$E_{ot} = 2P_t\tau$; $2P_t = 1.8$ W. $r_E = E_o^{PA}/E_o^{FDA} = M$ is the energy ratio per pulse and per beam position. $L_t = 2$dB is the TX loss, $L_a = 0.14$ dB is the atmospheric loss. The noise spectrum power density is $kT_s = 8.1 \times 10^{-18}$ mJ. A SW I target of radial length $L_{tg} = 2$ m, radial velocity $v_{tg} = -25.84$ m/s and radar cross section (RCS) $\sigma_s = 0.1\,\text{m}^2$ with a typical decorrelation time [7] $T_{ctg} = 100$ ms is considered. The total number of TX modules is $M \times N = 52$. Thus, for $a_m = 1$ the power per module is 17.31 mW.

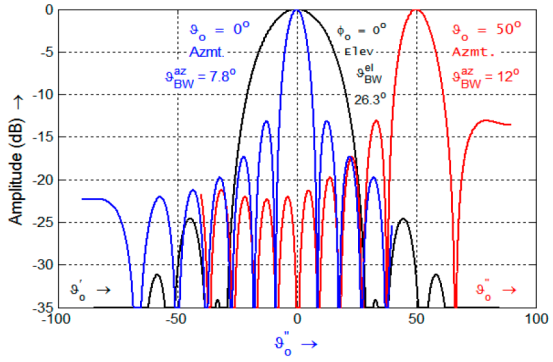

Fig. 9 *Antenna patterns with isotropic elements*

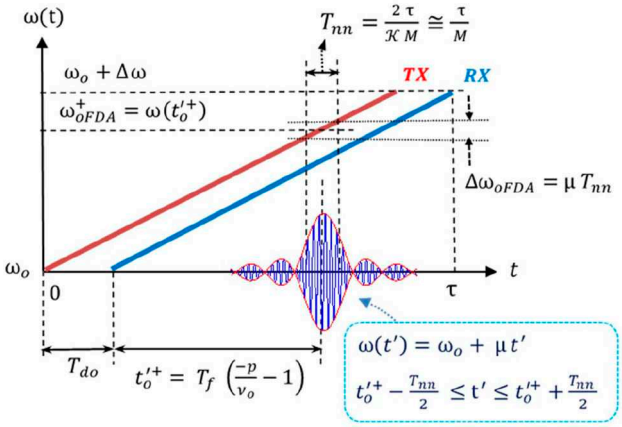

Fig. 10 *RF and bandwidth for a particular angle for + slope*

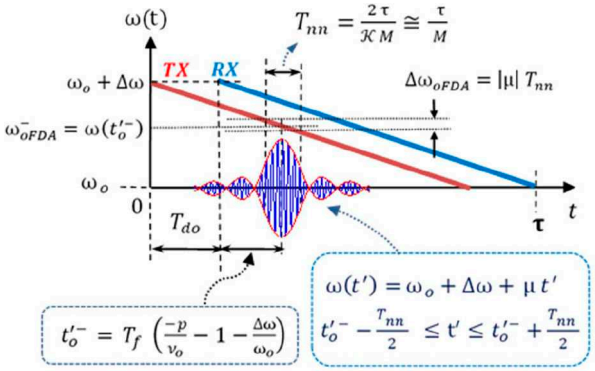

Fig. 11 *RF and bandwidth for a particular angle for – slope*

In TX modules the DDS oscillator outputs (S-band) should be up converted to f_o. In the RX modules down conversion and signal processing based on 2D $\mathcal{FT}$ should be combined with DBF. We need $N_b = 13$ RX beams to cover $N_b \vartheta_{BW}^{az} \cong 100°$ azimuth sector simultaneously. The FDA TX beam scans this sector in slow time T_p. In (17), $L_x = 3$ dB is the processing loss. I_n is the SNR improvement factor of cascaded single delay line canceller filter (DLCF) and DFL. v_{tg} and T_p are adjusted for the maximum $I_n = 8.53$. The DF shift is $f_{do} = 2.99$ kHz. The sampling frequency in T_p should be $f_s \geq 2 f_{bo}$. For a SW I target, $D_1 = \ell n(P_{fa})/\ell n(P_d) - 1$ is the detectability factor, where P_d is the probability of detection and P_{fa} is the probability of false alarm. The coherent integration interval with DLCF is $\text{CIT}^{\text{FDA}} = 22.26$ ms. The target should remain in ΔR_o during CIT^{FDA}, which leads to $L_{tg} \leq \Delta R_o - |v_{tg}|\text{CIT}^{\text{FDA}} = 3.32$ m. The frame time (FRT) is $\text{FRT}^{\text{FDA}} = n_-^{\text{FDA}}\text{CIT}^{\text{FDA}} = 468$ ms. The RCS of a SW I target will decorrelate $n_{ctg} = \text{FRT}^{\text{FDA}}/T_{ctg} = 5$ times in FRT^{FDA} providing a temporal diversity. We make a detection trial in each FRT^{FDA}, which is the cumulative detection step (CDS). In n_s^{FDA} CDS's we have

$$P_{cd}^{\text{FDA}} = 1 - (1 - P_d)^{n_s^{\text{FDA}}} \quad P_{cfa}^{\text{FDA}} = 1 - (1 - P_{fa})^{n_s^{\text{FDA}}} \tag{18}$$

For the chosen radar parameters, the solution of (17) gives $P_d = 0.9637$ for $P_{fa} = 0.5 \times 10^{-6}$ per CDS. Then, from (18) for $n_s^{\text{FDA}} = 2$, $P_{cd}^{\text{FDA}} = 0.9987$, and $P_{cfa}^{\text{FDA}} = 10^{-6}$.

In the FRT^{FDA} $\text{SNR}^{\text{FDA}} = 18.69$ dB and the non-coherent integration gain for $n_-^{\text{FDA}} = 21$ bursts and $\{P_d, P_{fa}\}$ per CDS is $G_i^{\text{FDA}} = 10.5$ dB. The diversity gain $G_{div}^{\text{FDA}} = 10.73$ dB stems from $n_{ctg} = 5$ and a two-fold ±slope frequency diversity amounting to $N_{div}^{\text{FDA}} = 2 \times 5 = 10$ diversity channels.

The build-up times (BUTs) for ± slopes are different causing different $f_{oFDA}^{\pm}$ centre frequency locations in the chirp. We have here $|f_{oFDA}^{+} - f_{oFDA}^{-}| > f_c$, where f_c is the decorrelation frequency of the SW I target given by $f_c \cong c/(2L_{tg}) = 75$ MHz. The local fBW at $f_{oFDA}^{\pm}$ is $\Delta f_{oFDA} \cong |\mu_f| T_{nn}/2 \cong 38.45$ MHz, where $T_{nn}/2 = 38.45\,\mu$s is the energy equivalent TBW. Since $\Delta f_{oFDA}(\pm) < f_c$ no intrapulse frequency diversity occurs due to Δf_{oFDA}. This makes the FDA waveform distortionless. The local TX/RX frequency locations and bandwidths for a specific angle and ± slopes are shown in Figs. 10 and 11. The final waveform time can be expressed by $T_{rv}^{\text{FDA}} = \text{WFT}^{\text{FDA}} = n_s^{\text{FDA}} \cdot \text{FRT}^{\text{FDA}} = 935$ ms.

5 Discussion and comparison with PA radar

The time on a target should be long enough for the full back scattering signal to be established. This condition may be expressed by $L_{tg} < L_{tgm} = (c/2)\vartheta_{BW}^{az}/|\Omega_\vartheta|$. From (13), for $\vartheta_o = \{0°,\ 50°\}$ and $\vartheta_{BW}^{az} = \{7.8°,\ 12°\}$, $L_{tgm} = \{5.1, 7.8\}$ km.

The effects of increasing some parameters are expressed as

$$\left.\begin{aligned} &\tau \uparrow \Rightarrow \{\mu_f, T_f, f_{BW}, f_{bo}\} \downarrow \quad \& \ \{T_{nn},\ E_o\} \uparrow \\ &T_\ell \uparrow \Rightarrow \{f_o, \Delta f,\ \eta\} \downarrow \quad \& \{\mu_f, T_f, \Delta R_o, f_{bo}\} \uparrow \\ &f_o \uparrow \Rightarrow \{T_f, T_{nn}, f_{BW}, f_{do}\} \uparrow \\ &M \uparrow \Rightarrow \{f_{BW},\ \Delta R_o, E_o, G_A\} \uparrow \ \& \{\ T_{nn}, \vartheta_{BW}^{az}\} \downarrow \end{aligned}\right\} \tag{19}$$

We shall compare the present FMCW/FDA radar with an equivalent FMCW/PA radar. The parameters of the PA radar other than those of the FDA radar are $N_-^{\text{PA}} = 8$, $n_-^{\text{PA}} = 4$, $n_s^{\text{PA}} = 1$, $\Delta f^{\text{PA}} = 38.46$ MHz. Then, we have the same $\Delta R_o = 3.897$ m. From burst-to-burst $N_{div}^{\text{PA}} = 4$-fold frequency agility steps, amounting to a frequency agility bandwidth of $\text{fBW} = 4 f_c = 300$ MHz, are used. In (17), the factor r_E is to be removed for PA. Then the solution of (17) for PA yields $P_d^{\text{PA}} = 0.9984$, $P_{fa}^{\text{PA}} = 10^{-6}$, $G_i^{\text{PA}} = 5.4$ dB, $G_{div}^{\text{PA}} = 17.98$ dB, $\text{CIT}^{\text{PA}} = 22.26$ ms and $\text{FRT}^{\text{PA}} = 89.0$ ms. We need $N_b = 13$ TX beam positions. The revisit time of a target is then given by $T_{rv}^{\text{PA}} = N_b \text{FRT}^{\text{PA}} = 1158$ ms with $\text{SNR}^{\text{PA}} = 24.7$ dB.

The total energy input to the array per pulse is $E_{oin} = E_{ot}$, which is the same in both cases. However, the total energy delivered in T_{rv}^{FDA} and T_{rv}^{PA} are different. We can show that

$$E_{oT}^{\text{FDA}} = E_{oin}\, N_-^{\text{FDA}}\, n_-^{\text{FDA}}\, n_s^{\text{FDA}} \tag{20}$$

$$E_{oT}^{\text{PA}} = E_{oin}\, N_-^{\text{PA}}\, n_-^{\text{PA}}\, n_s^{\text{PA}}\, N_b \tag{21}$$

$$E_{oT}^{\text{FDA}}/E_{oT}^{\text{PA}} = 0.807 \tag{22}$$

$$\left(E_{oT}^{\text{FDA}} \cdot T_{rv}^{\text{FDA}}\right)/\left(E_{oT}^{\text{PA}} \cdot T_{rv}^{\text{PA}}\right) = (0.807)^2 = 0.652 \tag{23}$$

It is thus observed that the present FDA radar has less energy-time product compared to the equivalent PA radar.

However, this conclusion cannot be generalised for all cases of comparison. Each pair of radar design should be evaluated separately on their own merits.

If we did not use a cumulative detection in the FDA radar, we would have $T_{\text{rv}}^{\text{FDA}} = 468\,\text{ms}$ with an $\text{SNR}^{\text{FDA}} = 18.7\,\text{dB}$.

In FRT target moves 12.1 and 29.9 m for FDA and PA radars, respectively. This property may be an advantage in FDA radar for tracking high RCS targets. The TX f_{oFDA} centre frequencies for each scanning angle due to different BUTs are different and remains within the fBW Δf^{FDA}. The radar frequency f_{o} agility in FMCW/FDA causes waveform agility. The FDA radar, as it distributes the energy to time and angle, has a low probability of intercept property.

6 Conclusions

The FMCW/FDA radar based on DDS technology offers interesting advantages such as narrow relative frequency bandwidth η, high-chirp delay T_ℓ between antenna elements and smaller f_{o} as large $f_{\text{o}}\,T_\ell$ is desired. Using the SO the $\mathcal{FT}$ domain signal processing can be performed conveniently. The time angle scanning property can be exploited by a cumulative detection scheme to compensate the reduced SNR inherent in all FDA-based radars. It is also shown by a fair comparison of equivalent FDA and PA radars that the total energy-time product to achieve the same P_{d}, P_{fa} is smaller for FDA radar than that for PA radar. It is also found that for short range and high RCS targets FDA radar is more advantageous.

7 Acknowledgements

The authors would like to thank Aselsan for the motivation and support given to this work.

8 References

[1] Antonik, P., Wicks, M.C., Griffiths, H.D., *et al.*: 'Frequency diverse array radars'. IEEE Radar Conf., USA, 2006, pp. 215–217

[2] Secmen, M., Demir, S., Hizal, A., *et al.*: 'Frequency diverse array antenna with periodic time modulated pattern in range and angle'. IEEE Radar Conf., USA, 2007, pp. 427–430

[3] Eker, A.T., Demir, S., Hizal, A.: 'Exploitation of linear frequency modulated continuous waveform LFMCW for frequency diverse arrays', *IEEE Trans. Antennas Propag.*, 2013, **61**, pp. 3546–3553

[4] Cetintepe, C.: 'Analysis of frequency diverse arrays for radar and communication applications'. PhD thesis, METU EEE Department, 2015

[5] Turhaner, A., Demir, S., Hizal, A.: 'Monopulse direction finding for linear frequency modulation based frequency diverse array'. IEEE Radar Conf., USA, 2017

[6] Khan, R.H., Power, D.: 'Doppler processing for coherent chirp radars', 1994 Proc. Canadian Conf. on Electrical and Computer Engineering, 1994, vol. 2, pp. 767–770

[7] Edrington, T.S.: 'The amplitude statistics of aircraft radar echoes', *IEEE Trans. Mil. Electron.*, 1965, **9**, (1), pp. 10–16